PCCP

Accepted Manuscript

ROYAL SOCIETY OF CHEMISTRY

www.rsc.org/pccp

Journal Name

ARTICLE TYPE

Cite this: DOI: 10.1039/xxxxxxxxxx

Layering Effects on Low Frequency Modes in *n*-layered MX_2 Transition Metal Dichalcogenides†

Antonio Cammarata,*[a] and Tomas Polcar[a,b]

Received Date
Accepted Date

DOI: 10.1039/xxxxxxxxxx

www.rsc.org/journalname

n-layered ($n = 2,3,4$) MX_2 transition metal dichalcogenides (M= Mo, W; X=S, Se, Te) have been studied with DFT techniques. Long-range van der Waals forces have been modeled with Grimme correction to capture the interlayer interactions. We study the dynamic and electronic dependence of atomic displacement from the number of layers. We find that the displacement patterns mainly affected by a change in the layer number are the low-frequency modes at Γ and A k-points; such modes are connected with the intrinsic tribological response. We disentangle the electro-phonon coupling by combining orbital polarization, covalency and cophonicity analysis with phonon band calculations. We find that the frequency dependence from the number of layers and the atomic type has a non-trivial relation with the electronic charge distribution in the interlayer region. We show that the interlayer electronic density can be adjusted by properly tuning the M-X cophonicity, acting as a knob to control the vibrational frequencies, hence the intrinsic frictional response. The present results can be exploited to study the electro-phonon coupling effects in TMD-based materials beyond tribological applications.

1 Introduction

Transition metal dichalcogenides (TMDs) are van der Waals structures with general MX_2 stoichiometry (M= transition metal cation, X= chalogen anion); they are attracting great interests because of their close features with graphene and their highly versatile stoichiometry.[1] Actual research focus is towards finite *n*-layer TMD systems, since they can be easily exfoliated and assembled into few free-standing atomic layers.[2–5] Numerous studies have dealt mainly with the electronic properties thanks to their application in photovoltaic devices, lithium ion batteries, hydrogen evolution catalysis, transistors and so on.[6–10] Only few theoretical works investigated on the tribologic aspects,[11–15] and, to the best of our knowledge, there are no theoretical studies about the electron-phonon coupling effects on the *intrinsic frictional properties* in *n*-layer TMDs. With the term *intrinsic friction* we refer to the friction generated by the relative motion of few adjacent atom layers in the absence of structural irregularities (dislocations, layer truncations etc.); it is thus the result of the local electronic and structural features of the material at the atomic level, originating only from the atomic type and the geometric arrangement of the atoms forming the structure. The knowledge of the intrinsic tribological properties is nowadays becoming mandatory with the advance of the experimental techniques, now capable to micromanipulate free-standing atomic layers.[16]

In the present work, we study the electro-vibronic coupling contributions to the lattice vibrations, e.g. *phonon modes*, that may facilitate interlayer slip, hence affecting intrinsic friction. In terms of the classical picture, we can think to each phonon mode as a periodic atomic motion about an equilibrium position due to a harmonic restoring force, to which it is associated a frequency ω such that

$$\omega = \sqrt{\frac{k_f}{m}} \tag{1}$$

where k_f is the force constant and m is the reduced mass of the atoms involved in the motion. The lower is ω, the weaker is the restoring force to which k_f is associated, and the higher is the amplitude of the corresponding atomic displacement at a fixed system energy. It is here worthy to recall that only few modes are related to the tribological conditions, corresponding to pure rigid layer translations or to layer shifts combined with intra-layer motions, like stretching and/or bending of atomic bonds or flattening of coordination polyhedra. Such layer shifts can be realized along a direction either parallel or orthogonal to the MX_2 sheets; the former are associated to the layer sliding, the latter correspond to variations of the interlayer distance and are thus related to the response to external load. Apart from such kinds of lattice vi-

[a] Department of Control Engineering, Czech Technical University in Prague, Technicka 2, 16627 Prague 6, Czech Republic. Fax: +420 224 91 8646; Tel: +420 224 35 7598; E-mail: cammaant@fel.cvut.cz

[b] nCATS, FEE, University of Southampton, SO17 1BJ Southampton, United Kingdom.

† Electronic Supplementary Information (ESI) available: Optimized structures of the bulk MX_2 model systems; definition of "in-phase" and "out-of-phase" layer shift. See DOI: 10.1039/b000000x/

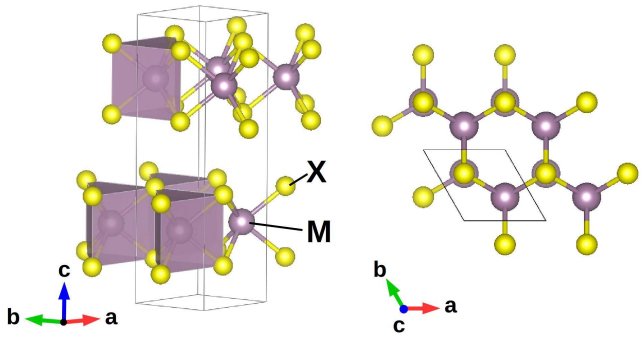

Fig. 1 Hexagonal $P6_3/mmc$ structure of 2H polymorph MX_2 crystal (M = transition metal, X = chalcogen atom). M–X bonds are arranged in a trigonal prismatic fashion, forming MX_2 layers that can reciprocally slide thanks to weak van der Waals interactions.

brations contributing to the intrinsic tribological response, other kinds of atomic displacement patterns are found; indeed, we find that only sliding and variable interlayer distance modes are those mostly affected by the number of layers. We here find that the origin of the mode frequency shift, as a function of the number of layers and the atomic type, resides in the interlayer electronic distribution; we then exploit the recently formulated cophonicity metric[17] to easily parameterize such distribution in terms of the atomic type. In this way, we find a way to disentangle the electro-vibronic coupling determining the mode frequency in finite TMD systems; at the same time, we obtain a guide to properly select the chemistry and the stoichiometry of the system to finely tune the vibrational frequencies. These outcomes can be promptly exploited to engineer the lattice dynamic properties and the electronic distribution in materials for diverse applications other than tribology, like in optical or electronic devices.

2 Methods

MX_2 transition metal dichalcogenides are layered structures, each layer formed by hexagonally packed metal atoms (M) coordinating six chalcogen anions (X) in a trigonal prismatic fashion (Figure 1); adjacent layers are bound by weak van der Waals forces allowing relative sliding under tribological conditions. Among the several stable TMDs polymorphs and polytypes that are found,[1] we choose the 2H polymorph crystalline MX_2 compounds as reference structure, with M=Mo, W and X=S, Se, Te and hexagonal $P6_3/mmc$ symmetry (SG 194); for simplicity, we will refer to them as MX by dropping the stoichiometric coefficients. The 2H configuration consists of two adjacent layers oriented in such a way that an M atom of one layer is aligned with two X atoms of the other one along the direction orthogonal to each layer (c-axis in our setting — see Figure 1); this geometric configuration has been found to correspond to the lowest energy value for several arrangements of two subsequent MoS_2 layers.[18] Starting from such reference geometries (see Electronic Supplementary Information), for each MX system, we truncate the periodic structure along the c axis and consider only 2, 3 and 4 MX_2 adjacent layers; we then apply the periodic boundary conditions and set the simulation box length along the c-axis at 65 Å, so as to prevent interactions between images of outer layers. In this way, for each MX system, we build 3 models that we name MX-nL, where n specifies the number of MX_2 layers present in the geometric configuration (Figure 2).

We perform density functional theory (DFT) calculations using the projector-augmented wave (PAW) formalism and the Perdew-Burke-Ernzerhof (PBE) energy functional[19] as implemented in VASP.[20] We also take into account Van der Waals interactions using the Grimme correction,[21] that is able to reproduce the structural features, as we reported in previous works.[17,22] The Brillouin zone is sampled with a minimum of a $7\times7\times5$ k-point mesh and plane wave cutoff of 700 eV. Full structural (atoms and lattice) relaxations are initiated from diffraction data[23–28] and the forces minimized to a 0.05 meV Å^{-1} tolerance. We computed the phonon band structure with the aid of the PHONOPY software,[29] using the finite displacement method.[30]

3 Results and Discussion

We are here interested on how the frequencies of intrinsic atomic displacements, i.e. *phonon modes*, change by varying the number n of MX_2 layers. We first relax the atomic positions of all the model systems and calculate the phonon band structure along a standard[31] linear path joining the high-symmetry points of the irreducible Brillouin zone (IBZ). We focus on the phonon modes calculated at the high-symmetry points of the IBZ, since, by suitable linear combinations, they can describe all the atomic displacement patterns.

We start the phonon analysis by observing that, irrespective of the M and X kind of atom, the mode frequencies mostly affected by the number of layers are the low-frequency modes at Γ and A k-points. In detail, such modes correspond to layer sliding and to layer displacements along the c-axis that change the interlayer distance; for simplicity, we name them as *sliding* modes and *variable interlayer distance* (variable ID) modes, respectively. The displacement patterns individuated in bi-layer systems ($n=2$) become more and more complex increasing the number of layers n: while the global character (sliding or variable ID) is preserved, new features peculiar of the number of layers appear, consisting mainly in in-phase and out-of-phase layer shifts (see Electronic Supplementary Information). It is worthy here to recall that we have already individuated[17,22] such distortion modes as relevant for the intrinsic tribological properties of the bulk material; we also discussed how it is possible to promote or hinder the layer sliding by controlling the corresponding vibrational frequencies. These displacement patterns, their associated frequencies and how they change upon external perturbation in the absence of structural defects depend on the electronic and structural features of the system, being thus *intrinsic* of the material.

No matter the character of the mode, out-of-phase layer displacements are associated to higher vibrational frequencies than the in-phase corresponding ones. Moreover, the out-of-phase mode frequencies increase with n, while opposite trend is observed for in-phase mode frequencies. To simplify our analysis, at fixed n, we will consider the average value of all the frequency modes pertaining to the sliding and variable ID modes. We will call $\omega_{\rm sl}(k)$ and $\omega_{\rm vID}(k)$ the average frequency of the sliding and variable ID mode frequencies, respectively, at fixed number n of layers and at a specific k-point of the IBZ.

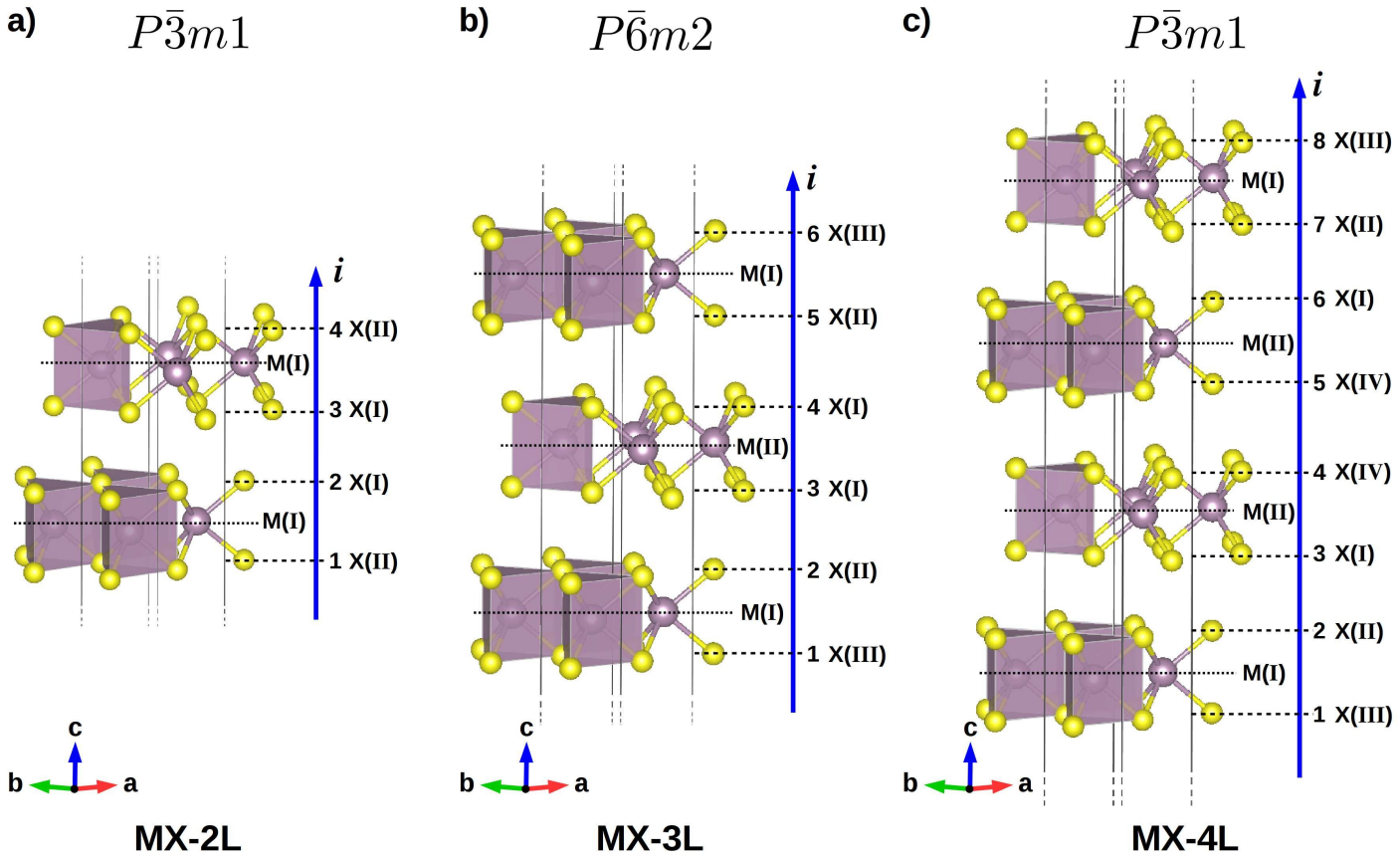

Fig. 2 MX periodic models are truncated along the c-axis direction in order to build the (a) trigonal $P\bar{3}m1$ (SG 164) MX-2L, (b) hexagonal $P\bar{6}m2$ (SG 187) MX-3L and (c) trigonal $P\bar{3}m1$ (SG 164) MX-4L systems, in which only 2, 3 and 4 MX_2 layers are present, respectively. Roman numbers in parenthesis indicate the kind of unique crystallographic site of the corresponding ion; all the M and X atoms, belonging to the same layer orthogonal to c-axis, occupy the same unique crystallographic position. X atom layers have been labeled as $i = 1, 2, 3\ldots$ following the c-axis direction orthogonal to them.

We observe that ω_{sl} and ω_{vID} frequencies have peculiar trend with n according to the chemical composition and the kind of k-point (Figure 3); we can only note that the trend is monotonic with the number of layers only for some of the considered chemistries. For this reasons, at this stage, no general rule can be stated about the dependency of the analized frequencies from n and the chemical composition; on the other hand, no clear trend can be extrapolated for the finite n-layered systems starting from the corresponding bulk structure, the former thus requiring specific investigation. We therefore need to find a way to parameterize the vibrational frequencies with some descriptors that are able to capture the electro-dynamic features governing the frequency shift at varying n and kind of M and X atoms. To this aim, we start by tracking the $C_{M,X}$ M–X bond covalency of all the systems at different n, making use of the bond covalency metric recently defined by means of atomic orbital contributions to the electronic density of states;[32] such metric is not specific of the kind of phenomenon under investigation, and has already been used to study various systems such as perovskite oxides,[32] optically active telluro-molybdates[33] and tribologic TMD materials.[17,22] We will group the M–X bonds according to their vicinity to the surface; we therefore call *outer* bonds those bonds belonging to the outermost MX_2 layers closest to the free surface of the system; we then refer to all the remaining ones as *inner* bonds. We first observe that outer bonds on the surface are more covalent than inner bonds; this is an expected result, since the absence of further layers above and below the free surface of the system favors the spread of the electronic density in the surface region. Bond covalency is nearly constant with the number of layers, with only the WSe and WTe systems showing the greatest $C_{M,X}$ variation with n. However, the covalency analysis does not reveal particular electronic characteristics relevant to parameterize the frequency change with n and the chemical composition. We thus need to investigate in deeper details the electronic distribution and how its features are responsible of the frequency shift.

The displacement patterns of the modes here considered, besides intralayer atomic motions, involve the relative shift of adjacent layer, either in the ab-plane (sliding) or along the c-axis (variable ID). Such motions are the results of interlayer interactions mainly mediated by the presence of electronic charge in the interlayer region; indeed, we already observed how the interlayer charge distribution is crucial to determine the stuctural response to external perturbations.[22] In this perspective, we measure the orbital polarization[34,35] of the X and M atomic species at different number of layers. Let's recall here that the orbital polarization

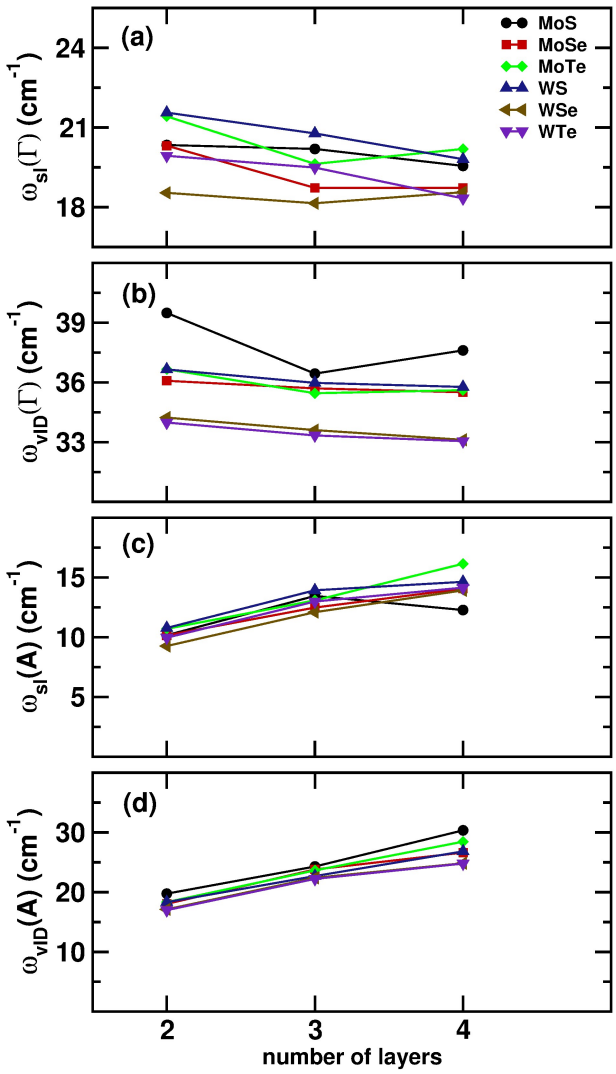

Fig. 3 Average frequency of sliding and variable ID modes at (a-b) Γ and (c-d) A point of the irreducible Brillouin zone as a function of the number of layers n. Trend is peculiar of the chemical composition and no general rule can be extrapolated.

$\mathscr{P}$ of m_{l1} orbital relative to m_{l2} orbital is defined as

$$\mathscr{P}_{l_1 m_{l1}, l_2 m_{l2}} = \frac{n_{l_1 m_{l1}} - n_{l_2 m_{l2}}}{n_{l_1 m_{l1}} + n_{l_2 m_{l2}}}, \qquad (2)$$

where $n_{l_1 m_{l1}}$ and $n_{l_2 m_{l2}}$ are the occupancies of $|l_1 m_{l1}\rangle$ and $|l_2 m_{l2}\rangle$ orbitals, with orbital quantum number l_i and magnetic quantum number m_{li}, respectively. It is an effective measure of the charge excess in the former orbital with respect to the latter: positive values indicate that m_{l1} orbital is more populated than m_{l2}, while opposite holds for negative values. Using real-space atomic orbital projections, it is possible to partition the electronic density into distinct atomic and interatomic regions, so as to isolate the single contributions hence identifying the features of the electronic distribution. In detail, for each studied system, we calculate $\mathscr{P}_{px-py}$, $\mathscr{P}_{px-pz}$ and $\mathscr{P}_{py-pz}$ of the X atom, and $\mathscr{P}_{t_{2g}-e_g}$ and $\mathscr{P}_{d_{x^2-y^2}-d_{z^2}}$ of the M cations. We first notice that M orbital polarization and $\mathscr{P}_{px-py}$ orbital polarization of X atom is nearly constant with n.

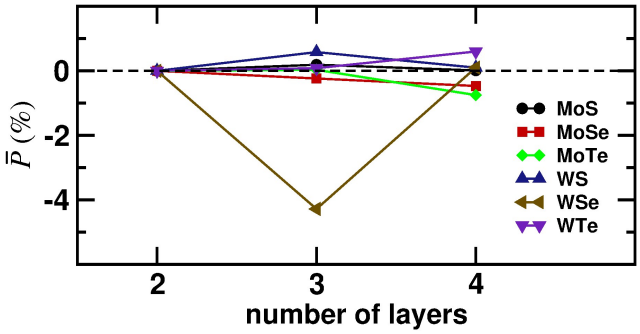

Fig. 4 Average orbital polarization difference $\overline{\mathscr{P}}$ as a function of the number of layers n. The electronic distribution represented by $\overline{\mathscr{P}}$ is peculiar of the chemical composition.

Moreover, $\mathscr{P}_{px-py}$ is small, this meaning that the charge distribution is uniform in each plane containing the X atoms and orthogonal to the c-axis (X layer), and is not significantly affected by n. Irrespective of the composition and the number of layers, $\mathscr{P}_{px-pz}$ and $\mathscr{P}_{py-pz}$ of the X layers below the surface (inner X layers) is higher than that of the X layers forming the surface of the system (outer X layers); this means that, compared to outer layers, in inner X layers charge tends to distribute on the plane containing the X atoms and orthogonal to the c axis. Moreover, $\mathscr{P}_{px-pz}$ and $\mathscr{P}_{py-pz}$ orbital polarizations are both negative, indicating excess of charge in the interlayer region with respect to the X layers; the actual value depends on the kind of M and X atoms and on the number of layers n.

The interactions between two adjacent layers is mediated by the interlayer charge distribution, that is the result of the charge contributions from two X layers facing across the interlayer gap. We observe that equivalent X crystallographic sites contribute to the interlayer charge density in equal manner; different contributions are found when the X crystallographic site pertaining to each of the two X layers are distinct. Such difference depends on the X species and on the number of layers n, that determines eventual distinctions between the Wyckoff positions of the X anions, and can be evaluated considering both $\mathscr{P}_{px-pz}$ and $\mathscr{P}_{py-pz}$. For this reason, we are going to focus on the *average orbital polarization difference* $\overline{\mathscr{P}}$ that we define as

$$\overline{\mathscr{P}} = \frac{1}{2}\left[(\mathscr{P}^{i+1}_{px-pz} - \mathscr{P}^{i}_{px-pz}) + (\mathscr{P}^{i+1}_{py-pz} - \mathscr{P}^{i}_{py-pz})\right], \qquad (3)$$

where i is the X layer label counted innerwards from the surface along the c axis (see Figure 2). By inspecting Equation 3, we can appreciate that $\overline{\mathscr{P}}$ is a measure of the electronic charge distributed between the i-th and the $i+1$-th layers, as it is a function of the orbital polarizations involving the X atoms and their p_z orbitals that point towards the $i/i+1$ interlayer region. Thanks to the symmetries of the systems, we need to evaluate $\overline{\mathscr{P}}$ only for $i = 2$ and for $n = 2,3$; in particular, $\overline{\mathscr{P}} = 0$ in all bi-layer systems, since X atoms in layers labeled with $i = 2$ and $i = 3$ occupy the same crystallographic position X(I).

We first notice that, except in WSe-3L system, $\overline{\mathscr{P}}$ values are similar. This exception could be due to W-Se intralayer interactions specific of the atomic kind forming the W-Se bond, and

the geometric symmetries pertaining to the 3-layer configuration (Space Group $P\bar{6}m2$). However, none of the electronic and vibrational analyses we perform in this work show particular exceptions relative to the WSe system, and all the observed quantities vary smoothly with the number of layers. For this reason, at this stage, we do not have enough information to describe the mechanism at the atomic scale that produces the interlayer charge distribution, hence $\overline{\mathscr{P}}$, specific of the WSe-3L system. Nonetheless, we are here concerned to find a way on how to relate the vibrational frequencies to some property of the system (atomic species, geometric distortions) that is experimentally accessible, in order to control the lattice dynamics *via* external parameters. We therefore consider the WSe-3L $\overline{\mathscr{P}}$ value as peculiar of that system and limit our considerations to the trend of $\overline{\mathscr{P}}$ against the number of layers, postponing further investigations on it to future works. We also observe that the trend of $\overline{\mathscr{P}}$ *vs* n is peculiar of the chemical composition (Figure 4); then, we relate ω_{sl} and ω_{vID} to the corresponding $\overline{\mathscr{P}}$ values (Figure 5). The vibrational frequencies have non-trival dependence from $\overline{\mathscr{P}}$; in general, $\overline{\mathscr{P}} \approx 0$ realizes the highest and lowest frequency values at Γ and A points, respectively. This means that whenever two X sheets contribute in the same amount to the charge density of the interlayer region that separates them, the Γ and A mode frequencies are the highest and the lowest achievable, respectively. We want to stress here that we have found a relation between the average orbital polarization difference $\overline{\mathscr{P}}$ and the mode frequency ω by varying the number of layers n at fixed MX_2 composition; nonetheless, such relation does not contain any information on the number of layers present in the system, since n does not enter in the expression for $\overline{\mathscr{P}}$. This tells us that, once the system is completely defined by fixing chemical composition and number of layers, the interlayer charge distribution is fixed and determines the vibrational frequencies. We can then adjust ω by varying $\overline{\mathscr{P}}$. However, ω is a non trivial function of $\overline{\mathscr{P}}$ that, in turn, has a complex dependence from the number of layers and the chemical composition.

The ω-$\overline{\mathscr{P}}$ relation clearly indicates that the vibrational frequencies are coupled with the electronic distribution in the interlayer region; thanks to this coupling, we can relate $\overline{\mathscr{P}}$ to the atomic contributions to the phonon density of states, hence, to the atomic type. To do this, we now make use of the *cophonicity* dynamical descriptor,[17] that is able to capture the relative atomic contribution to a specific phonon band.

We evaluate the cophonicity C_{ph}(M-X) of the M-X pair in all the systems in the frequency range $[0,54]$ cm^{-1}, corresponding to the band of the ω_{sl} and ω_{vID} frequencies that we are considering. We then relate C_{ph}(M-X) to $\overline{\mathscr{P}}$ and find a simple relation between the average orbital polarization difference and the M-X pair cophonicity (Figure 6). Such relation is the result of the electron-phonon coupling in the studied systems. Except for the WSe system, the C_{ph}(M-X) *vs* $\overline{\mathscr{P}}$ trend suggests a linear relation between the two quantities; however, further analysis on geometries including a higher number of layers is required to confirm or discard the linear trend hypothesis. We observe that small changes of the M-X cophonicity can induce large variations on $\overline{\mathscr{P}}$, that is, on the charge density present in the interlayer region. Since ω_{sl} and ω_{vID} vibrational frequencies depend on the interlayer electronic distribution, that in turn depends on cophonicity, the M-X pair cophonicity can be used to tune the vibrational fre-

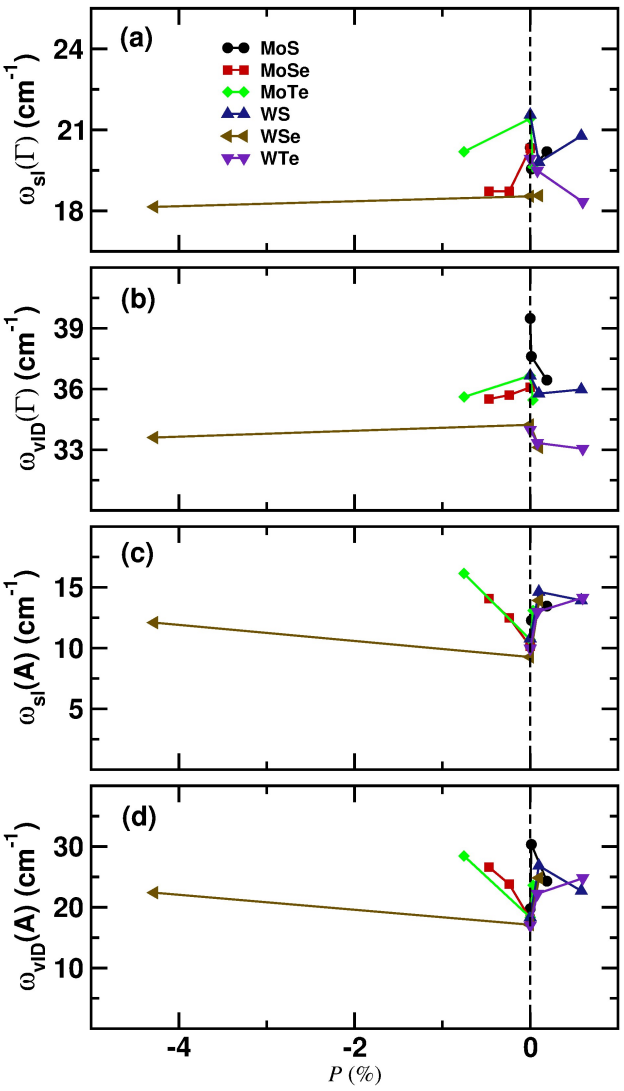

Fig. 5 Average frequency of sliding and variable ID modes at (a-b) Γ and (c-d) A point of the irreducible Brillouin zone as a function of the average orbital polarization difference $\overline{\mathscr{P}}$. The highest and lowest frequency values at Γ and A points are realized at $\overline{\mathscr{P}} \approx 0$.

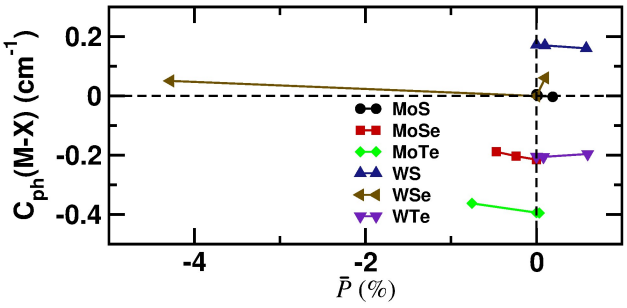

Fig. 6 Cophonicity of the M-X pair as a function of the average orbital polarization difference. The simple relation can be exploited for a direct control of the phonon frequencies.

quencies. An important result is that, unlike the ω-$\overline{\mathscr{P}}$ relation, $\overline{\mathscr{P}}$ seems to vary smoothly with cophonicity; this suggests that cophonicity is a promising descriptor to tune the interlayer charge, hence the related lattice dynamics. We already noticed that, in general, $\overline{\mathscr{P}} \approx 0$ maximises and minimises the Γ and A frequencies, respectively; data shown in Figure 6 suggests that, depending on the atomic type of the X anion, cophonicity must be increased (X=S) or decreased (X=Se, Te) in order that $\overline{\mathscr{P}}$ approaches zero and the vibrational frequencies tend to critical values (maxima or minima). In previous works,[17,22] we already observed that the cophonicity depends on the M and X atomic types, the geometry of the system and the electronic density distribution; indeed, the cophonicity descriptor captures several entangled properties that can be singularly adjusted to finely tune the M-X cophonicity value. Chemical composition and stoichiometry can be chosen in such a way as to induce specific structural distortions that alter the electronic distribution; this latter, in turn, alters the interatomic interactions that determine the vibrational motions of the system. We can thus conclude that the cophonicity of the system can be exploited as a knob to control the phonon frequencies in n-layered MX_2 TMDs. In our previous studies on TMDs,[17,22] we provide a protocol on how to adjust the system cophonicity to tune the phonon frequencies, that allowed us to identify a new TMD-derived phase which is expected to have enhanced intrinsic frictional response.

In the present study we have shown that the vibrational frequencies depend on the number of layers and on the chemical composition in such a way that they cannot be parameterized through a simple relation with the corresponding electronic distribution. Nonetheless, we find that the electro-stuctural coupling can be described by a simple relation between the charge density of the interlayer region and the cophonicity of the system. Once n is fixed, the cophonicity value, hence the electro-structural coupling, can be adjusted by changing the chemical composition; in this way, it is possible to finely tune the vibrational frequencies of the system. As a final comment, we note that this feature can also be exploited to adjust the charge density in the interlayer region in TMDs used in electronic or optical devices based on 2D layered structures.

4 Conclusions

We studied the intrinsic tribological response of n-layered ($n = 2,3,4$) MX_2 transition metal dichalcogenides with DFT techniques. The frequencies mostly affected by the number of layers are those associated to the low-frequency modes at Γ and A k-points of the irreducible Brillouin zone; such modes are connected with the intrinsic tribological response. We find that the charge distribution in the interlayer region is crucial in determining the phonon frequency; however, the electronic density displays a complex dependence from the number of layers and the atomic type. Nonetheless, we show that there exists a simple relation between the M-X cophonicity and the average orbital polarization difference representing the interlayer charge distribution. In particular, despite further investigations are required, we are confident that, according to the X atomic type, cophonicity must be increased or decreased in order that $\overline{\mathscr{P}} \approx 0$ and the vibrational frequencies tend to critical values. Such relation is the result of the electro-vibrational coupling. The electron-phonon coupling can be exploited to control the vibrational frequencies of the system: by tuning the cophonicity value, we can control the intelayer charge density hence the vibrational frequencies at fixed number of layers. This feature can be exploited to tune the electronic charge distribution in TMD-based devices for applications beyond tribology.

5 Acknowledgements

This work has been done with the support of inter-sectoral mobility and quality enhancement of research teams at Czech Technical University in Prague, CZ.1.07/2.3.00/30.0034. This work was supported by the IT4Innovations Centre of Excellence project (CZ.1.05/1.1.00/02.0070), funded by the European Regional Development Fund and the national budget of the Czech Republic via the Research and Development for Innovations Operational Programme, as well as Czech Ministry of Education, Youth and Sports via the project Large Research, Development and Innovations Infrastructures (LM2011033). The use of VESTA[36] software is also acknowledged.

References

1 M. Chhowalla, H. S. Shin, G. Eda, L.-J. Li, K. P. Loh and H. Zhang, *Nat. Chem.*, 2013, **5**, 263–275.

2 P. Browning, S. Eichfeld, K. Zhang, L. Hossain, Y.-C. Lin, K. Wang, N. Lu, A. R. Waite, A. A. Voevodin, M. Kim and J. A. Robinson, *2D Materials*, 2015, **2**, 014003.

3 A. L. Elías, N. Perea-López, A. Castro-Beltrán, A. Berkdemir, R. Lv, S. Feng, A. D. Long, T. Hayashi, Y. A. Kim, M. Endo, H. R. Gutiérrez, N. R. Pradhan, L. Balicas, T. E. Mallouk, F. López-Urías, H. Terrones and M. Terrones, *ACS Nano*, 2013, **7**, 5235–5242.

4 R. Lv, J. A. Robinson, R. E. Schaak, D. Sun, Y. Sun, T. E. Mallouk and M. Terrones, *Accounts of Chemical Research*, 2015, **48**, 56–64.

5 Y. Gong, J. Lin, X. Wang, G. Shi, S. Lei, Z. Lin, X. Zou, G. Ye, R. Vajtai, B. I. Yakobson, H. Terrones, M. Terrones, B. Tay, J. Lou, S. T. Pantelides, Z. Liu, W. Zhou and P. M. Ajayan, *Nat Mater*, 2014, **13**, 1135–1142.

6 X. Zhang, X.-F. Qiao, W. Shi, J.-B. Wu, D.-S. Jiang and P.-H. Tan, *Chem. Soc. Rev.*, 2015, **44**, 2757–2785.

7 R. Roldán, J. A. Silva-Guillén, M. P. López-Sancho, F. Guinea, E. Cappelluti and P. Ordejón, *Annalen der Physik*, 2014, **526**, 347–357.

8 H. Sahin, S. Tongay, S. Horzum, W. Fan, J. Zhou, J. Li, J. Wu and F. M. Peeters, *Phys. Rev. B*, 2013, **87**, 165409.

9 H. Terrones, E. D. Corro, S. Feng, J. M. Poumirol, D. Rhodes, D. Smirnov, N. R. Pradhan, Z. Lin, M. A. T. Nguyen, A. L. Elías, T. E. Mallouk, L. Balicas, M. A. Pimenta and M. Terrones, *Scientific Reports*, 2014, **4**, 4215 EP –.

10 Y.-H. Zhao, F. Yang, J. Wang, H. Guo and W. Ji, *Scientific Reports*, 2015, **5**, 8356 EP –.

11 S. Cahangirov, C. Ataca, M. Topsakal, H. Sahin and S. Ciraci, *Phys. Rev. Lett.*, 2012, **108**, 126103.

12 T. Onodera, Y. Morita, A. Suzuki, M. Koyama, H. Tsuboi, N. Hatakeyama, A. Endou, H. Takaba, M. Kubo, F. Dassenoy, C. Minfray, L. Joly-Pottuz, J.-M. Martin and A. Miyamoto, *J. Phys. Chem. B*, 2009, **113**, 16526–16536.

13 T. Onodera, Y. Morita, R. Nagumo, R. Miura, A. Suzuki, H. Tsuboi, N. Hatakeyama, A. Endou, H. Takaba, F. Dassenoy, C. Minfray, L. Joly-Pottuz, M. Kubo, J.-M. Martin and A. Miyamoto, *J. Phys. Chem. B*, 2010, **114**, 15832.

14 T. Liang, W. G. Sawyer, S. S. Perry, S. B. Sinnott and S. R. Phillpot, *Phys. Rev. B*, 2008, **77**, 104105.

15 Y. Morita, T. Onodera, A. Suzuki, R. Sahnoun, M. Koyama, H. Tsuboi, N. Hatakeyama, A. Endou, H. Takaba, M. Kubo, C. A. D. Carpio, T. Shin-yoshi, N. Nishino, A. Suzuki and A. Miyamoto, *Appl. Surf. Sci.*, 2008, **254**, 7618 – 7621.

16 J. P. Oviedo, S. KC, N. Lu, J. Wang, K. Cho, R. M. Wallace and M. J. Kim, *ACS Nano*, 2015, **9**, 1543–1551.

17 A. Cammarata and T. Polcar, *Inorganic Chemistry*, 2015, **54**, 5739–5744.

18 G. Levita, A. Cavaleiro, E. Molinari, T. Polcar and M. C. Righi, *J. Phys. Chem. C*, 2014, **118**, 13809–13816.

19 J. P. Perdew, K. Burke and M. Ernzerhof, *Phys. Rev. Lett.*, 1996, **77**, 3865–3868.

20 (*a*) G. Kresse and J. Furthmüller, *Comp. Mater. Sci.*, 1996, **6**, 15 – 50; (*b*) G. Kresse and D. Joubert, *Phys. Rev. B*, 1999, **59**, 1758–1775.

21 S. Grimme, *J. Comp. Chem.*, 2006, **27**, 1787–1799.

22 A. Cammarata and T. Polcar, *RSC Adv.*, 2015, **5**, 106809–106818.

23 B. Schönfeld, J. J. Huang and S. C. Moss, *Acta Crystallogr. B*, 1983, **39**, 404–407.

24 V. Kalikhman, *Inorg. Mater.*, 1983, **19**, 957–962.

25 L. Brixner, *J. Inorg. Nucl. Chem.*, 1962, **24**, 257 – 263.

26 W. Schutte, J. D. Boer and F. Jellinek, *J. Solid State Chem.*, 1987, **70**, 207 – 209.

27 V. L. Kalikhman, *Neorganicheskie Materialy*, 1983, **19**, 1060 – 1065.

28 A. A. Yanaki and V. A. Obolonchik, *Inorg. Mater.*, 1973, **9**, 1855–1858.

29 A. Togo, F. Oba and I. Tanaka, *Phys. Rev. B*, 2008, **78**, 134106.

30 (*a*) L. Chaput, A. Togo, I. Tanaka and G. Hug, *Phys. Rev. B*, 2011, **84**, 094302; (*b*) K. Parlinski, Z. Q. Li and Y. Kawazoe, *Phys. Rev. Lett.*, 1997, **78**, 4063–4066.

31 W. Setyawan and S. Curtarolo, *Comp. Mater. Sci*, 2010, **49**, 299 – 312.

32 A. Cammarata and J. M. Rondinelli, *J. Chem. Phys.*, 2014, **141**, 114704.

33 A. Cammarata, W. Zhang, P. S. Halasyamani and J. M. Rondinelli, *Chemistry of Materials*, 2014, **26**, 5773–5781.

34 A. Cammarata and J. M. Rondinelli, *Phys. Rev. B*, 2013, **87**, 155135.

35 M. J. Han, C. A. Marianetti and A. J. Millis, *Phys. Rev. B*, 2010, **82**, 134408.

36 K. Momma and F. Izumi, *J. Appl. Cryst.*, 2008, **41**, 653–658.